Reduced voltage sensitivity in a K^+-channel voltage sensor by electric field remodeling

Vivian González-Pérez[a,b], Katherine Stack[a], Katica Boric[a,b], and David Naranjo[a,1]

[a]Centro Interdisciplinario de Neurociencia de Valparaíso and Departamento de Neurociencia, Universidad de Valparaíso, Valparaíso 2349400, Chile; and [b]Programa de Doctorado en Ciencias Mención Neurociencia, Facultad de Ciencias, Universidad de Valparaíso, Valparaíso 2349400, Chile

Communicated by Ramón Latorre, Centro de Neurociencias, Universidad de Valparaíso, Valparaíso, Chile, January 25, 2010 (received for review November 4, 2009)

Propagation of the nerve impulse relies on the extreme voltage sensitivity of Na^+ and K^+ channels. The transmembrane movement of four arginine residues, located at the fourth transmembrane segment (S4), in each of their four voltage-sensing domains is mostly responsible for the translocation of 12 to 13 e_o across the transmembrane electric field. Inserting additional positively charged residues between the voltage-sensing arginines in S4 would, in principle, increase voltage sensitivity. Here we show that either positively or negatively charged residues added between the two most external sensing arginines of S4 decreased voltage sensitivity of a Shaker voltage-gated K^+-channel by up to ≈50%. The replacement of Val363 with a charged residue displaced inwardly the external boundaries of the electric field by at least 6 Å, leaving the most external arginine of S4 constitutively exposed to the extracellular space and permanently excluded from the electric field. Both the physical trajectory of S4 and its electromechanical coupling to open the pore gate seemed unchanged. We propose that the separation between the first two sensing charges at resting is comparable to the thickness of the low dielectric transmembrane barrier they must cross. Thus, at most a single sensing arginine side chain could be found within the field. The conserved hydrophobic nature of the residues located between the voltage-sensing arginines in S4 may shape the electric field geometry for optimal voltage sensitivity in voltage-gated ion channels.

action potential | charge hydration | Shaker | limiting slope | cysteine accessibility

The exquisite voltage sensitivity of voltage-sensitive Na^+ and K^+ channels proteins is due to their ability to translocate up to 12 to 13 tethered charge equivalents across the transmembrane electric field (1, 2). These charges must move electrophoretically across the transmembrane low dielectric environment for voltage-sensitive activation of ion conduction. In principle, the higher the net number of charges crossing the electric field in the voltage-sensing structure, the higher would be the voltage sensitivity. Nevertheless, such higher voltage sensitivity would imply more charges coming in contact with the low dielectric environment. Thus, evolutionary optimization of the voltage-sensing structure must be intimately related to the mechanisms of transmembrane charge stabilization.

The voltage-sensing structure in most known voltage-sensing membrane proteins is the voltage sensor domain (VSD). Voltage-gated ion channels contain four VSD in a tetra- or pseudo-tetrasymmetric disposition around the ion conduction pore structure. Each VSD is made of four transmembrane helical segments (S1–S4), with S4 being unusually charged in a highly conserved sequence array of six to eight basic amino acids periodically spaced by two hydrophobic residues (Fig. 1*A*). By neutralizing individual basic residues in the Shaker K-channel's S4, the four outermost arginines (R1–R4) have been identified as the main voltage-sensitive residues (1, 2). How these arginines are stabilized at the core of this unusually charged transmembrane segment and how they sense and move down the electric field are actively debated issues. Charged arginine side chains could be stabilized by a hydration shell protruding into the core of the membrane (3–7) or by countercharges located in the core of the protein (8, 9) or by phosphate groups of the polar head of phospholipids (9–15). Regardless of the stabilization mechanism, if an additional positively or negatively charged side chain is inserted between the voltage-sensing arginines of S4, it would move with them across the electric field during voltage sensing, producing a change in voltage sensitivity congruent with the sign of the charge and with the trajectory of S4.

After adding charged thiol adducts to cysteines individually placed at several charged and hydrophobic positions of the S4 of Shaker K-channels, Ahern and Horn (16) measured directly their effect on the total charge displaced during activation. Only the modification at the positions of the voltage-sensing arginines produced changes in the total charge congruent with the sign of the added adduct. In the other accompanying hydrophobic positions results were not as congruent, implying possible structural alterations or distortions in the electric field.

In the Shaker K^+ channel, we replaced by arginine (+1) or glutamate (−1) Val363 and Ile364, conserved hydrophobic positions located between R1 and R2 (Arg362 and Arg365; Fig. 1 *A* and *B*) (17, 18). We show here that these charge additions, either positive or negative, decreased channel voltage sensitivity by up to ≈50%. A detailed analysis of the charged variants of 363 showed that this residue, together with R1, became externally exposed, regardless of the activation state of the channel. We propose that the additional charged side chain displaces the external boundaries of the electric field inwardly, excluding R1 from voltage sensing. We suggest that, in the conserved array of arginines every two hydrophobic residues in S4, the arginine side chains are dedicated to sense the voltage (16), whereas the hydrophobic residues shape the electric field for optimal voltage sensitivity in voltage-gated ion channels.

Results

Charging the Side Chain of Residue 363 Reduces the Voltage Sensitivity by Half. Both mutations V363R and V363D were introduced in non–N-type inactivating and highly charybdotoxin-sensitive Shaker K^+ channel (*wt*) (19). Measured with the two-electrode voltage-clamp technique (TEVC) (20), both mutants showed levels of functional expression in *Xenopus* oocytes comparable to *wt*. As expected, both charge additions altered voltage dependence, although mildly (Fig. 1 *C–E*). The half-activation voltages ($V_{1/2}$) moved by similar magnitude but in opposite directions with respect to *wt*: $\Delta V_{1/2} = -17$ mV for V363D and $\Delta V_{1/2} = +11$ mV for V363R (Fig. 1*F*). These nearly symmetric shifts around *wt* suggest an unexpected small energetic impact on the closed–open equilibrium ($\Delta V_{1/2} \approx -3$ mV corresponds to ≈0.2 kcal/mol per

Author contributions: V.G.-P., K.S., K.B., and D.N. designed research; V.G.-P., K.S., K.B., and D.N. performed research; V.G.-P., K.S., and D.N. analyzed data; and V.G.-P. and D.N. wrote the paper.

The authors declare no conflict of interest.

[1]To whom correspondence should be addressed. E-mail: david.naranjo@uv.cl.

This article contains supporting information online at www.pnas.org/cgi/content/full/1000963107/DCSupplemental.

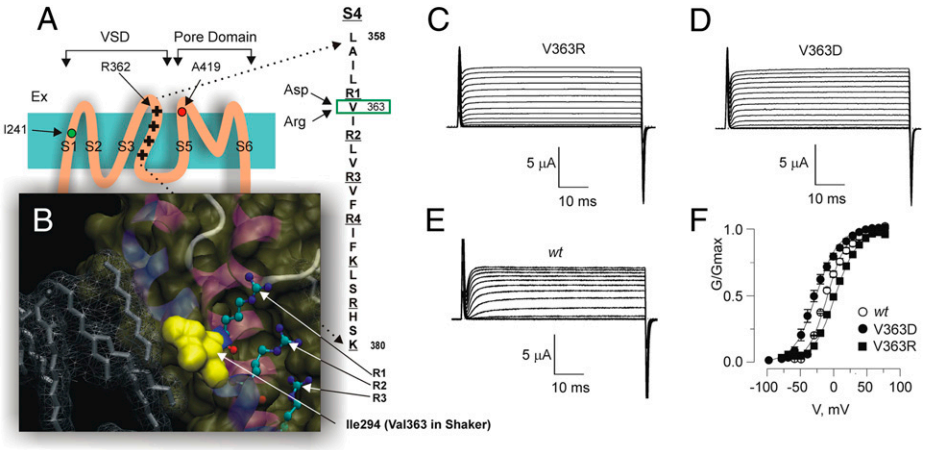

Fig. 1. Macroscopic currents of Shaker mutants carrying a charged side chain at position 363. (*A*) Topological representation of a single Shaker subunit. The S4 sequence is expanded at the right, where R1–R4 are underlined and 363 is enclosed by the green box. The proximity of R1 to 419, instead of 241, makes this drawing more closely represent the activated state. (*B*) Detail of segment S4 of the Kv1.2-Kv2.1 paddle chimera (PDB:2R9R) (10). R1, R2, and R3 are shown in ball-and-stick representation, Leu294 (equivalent to Shaker's Val363) is in solvent-accessible surface (yellow), and lipids are in wireframe representation (PGW501 and PGW503). Transmembrane S1 and S2 were removed for clarity. Molecular graphics made by VMD (http://www.ks.uiuc.edu/Research/vmd/). (*C–E*) TEVC currents evoked by voltage pulses incremented by 10 mV from a holding potential of −90 mV. (*F*) Normalized conductances vs. voltage (G-V relationship). We used the expression $G = I_K/(Vm - E_K)$ to calculate conductance, G, at each voltage, where I_K is the ionic K-current, Vm is the voltage pulse, and E_K, the reversal potential for K+, is assumed to be −90 mV. Results are means ± SE. Data points were fit to a simple Boltzmann distribution function with parameters $V_{1/2}$ = 1.9 mV, z = 1.53 e_o for V363R (n = 6); $V_{1/2}$ = −26.6, z = 1.53 e_o for V363D (n = 4); and $V_{1/2}$ = −9.5 mV, z = 1.76 e_o for *wt* (n = 5).

subunit) that stands in contrast to the dramatic change in the nature of the side chain from hydrophobic to charged (*Discussion*).

We tested whether its newly charged side chain contributed to the channel voltage sensitivity. The net number of moving charges required to activate the channels was measured with the limiting slope method with on-cell macropatch-clamp recordings (2, 21–23). This method estimates the effective valence of opening (z) at a voltage range where the open probability (Po) is so small that any opening represents channels climbing across the entire activation pathway in a single excursion. In Shaker, this condition is reasonably fulfilled experimentally at Po $<10^{-3}$ by measuring single-channel activity in membrane patches containing several hundred channels (23). In a typical experiment we counted the number of channels in the patch through nonstationary fluctuation analysis (23) (Fig. 2*A*); then, in the same patch, we recorded unitary openings to measure the absolute Po (22–24) (Fig. 2*B*). Preservation of the gating mechanism in the mutants was verified by fitting a single exponential function to the single-channel open-duration event distributions over a wide voltage interval (Fig. 2*C*). We estimated z by fitting the expression $Po = e^{zV/25}$ to the data within the interval $10^{-7} < Po < 10^{-3}$ (Fig. 2*D*). In dramatic contrast to *wt* (z = 12.1 ± 0.9 e_0), the additional charge at 363 halved the effective valence of opening regardless of its sign (Fig. 2*E*) (z = 6.0 ± 1.0 e_0 for V363R and z = 6.9 ± 1.2 e_0 for V363D). Similarly, for I364D and I364R z = 9.0 ± 0.5 and z = 5.3 ± 1.0 e_0, respectively (Fig. S1).

If S4 moves across the membrane as part of a rigid "paddle" during activation (25), an extra positive side chain should increase the valence, the opposite outcome of our findings. Additionally, although some rotational trajectories of S4 predict a reduced sensitivity (26), no proposed trajectory predicts similar amounts of reduction in z regardless of the sign of the charge at 363/364 side chain. This anomalous behavior could be due to modifications to the channel activation pathway or to the shape of the electric field across the voltage sensor. Here, we tested these hypotheses for the charged variants at 363.

Channel Opening Remains Tightly Coupled to Voltage Sensor Movement. Unlike *wt*, the charged 363 mutant channels could open before the physical excursion of S4 is completed, demanding the appearance of new voltage-dependent open conformations to account for the missing charge. The charge moving between open conformations (z ≈ 6) should produce a ≈10-fold duration change in the 10-mV interval shown in Fig. 2*C*. However, as for *wt*, both charge variants showed a single voltage-independent monodistributed single-channel open duration. Additionally, the charge–voltage (Q-V) relationships, measured with gating currents in the presence of 1 μM charybdotoxin (19, 20), retained their −40-mV displacement from the conductance–voltage (G-V) relationship (Fig. S2). Together, these findings are inconsistent with a weaker electromechanical coupling in the charged 363 variants.

Physical Excursion of S4 Remains Unchanged. Decreased voltage sensitivity would result if the mutant S4 travels a smaller physical distance during activation. At rest, R362 (R1) in S4 is in atomic proximity to I241 in S1 (27) and is near A419 in S5 in the activated channel (Fig. S3) (28, 29). In the mutant channels S4 would fail to ferry R1 between I241 and A419 during activation. To test this idea, we introduced cysteine pairs R1C/241C (Fig. S3*B*) and R1C/419C (Fig. S3*C*) to *wt* and its charged 363 variants. Inconsistent with such a reduced physical excursion of S4, all variants spontaneously formed disulfide bonds and, after reduction with DTT, were able to coordinate Cd^{2+} with micromolar affinity.

External Boundaries of the Electric Field Are Relocated. A charged side chain at 363 could relocate the external boundaries of the dielectric interfaces. In an outward relocation (hypothesis *i* in Fig. 3), a similar physical movement of S4 would scan a smaller fraction of the field. Meanwhile, an inward relocation (hypothesis *ii* in Fig. 3) would exclude part of S4 from the field, reducing the number of charges moving across. Replacing either R1 or R2 for cysteine (R1C or R2C) causes activation-dependent accessibility to the externally applied membrane impermeant thiol reagent methanethiosulfonate-ethyl-trimethylammonium (MTSET; Fig. 3, *Native*) (30, 31). Hypothesis *i* predicts that R1C and R2C would retain activation-dependent accessibility but be decreased overall. In contrast, hypothesis *ii* demands activation independent—and high—accessibility for R1C and/or R2C. To assay activation-dependent accessibility to external MTSET, we devised two separate voltage pulse protocols yielding a ≈10-fold difference in the overall channel Po (31). Channels were opened every 2 s by positive pulses lasting

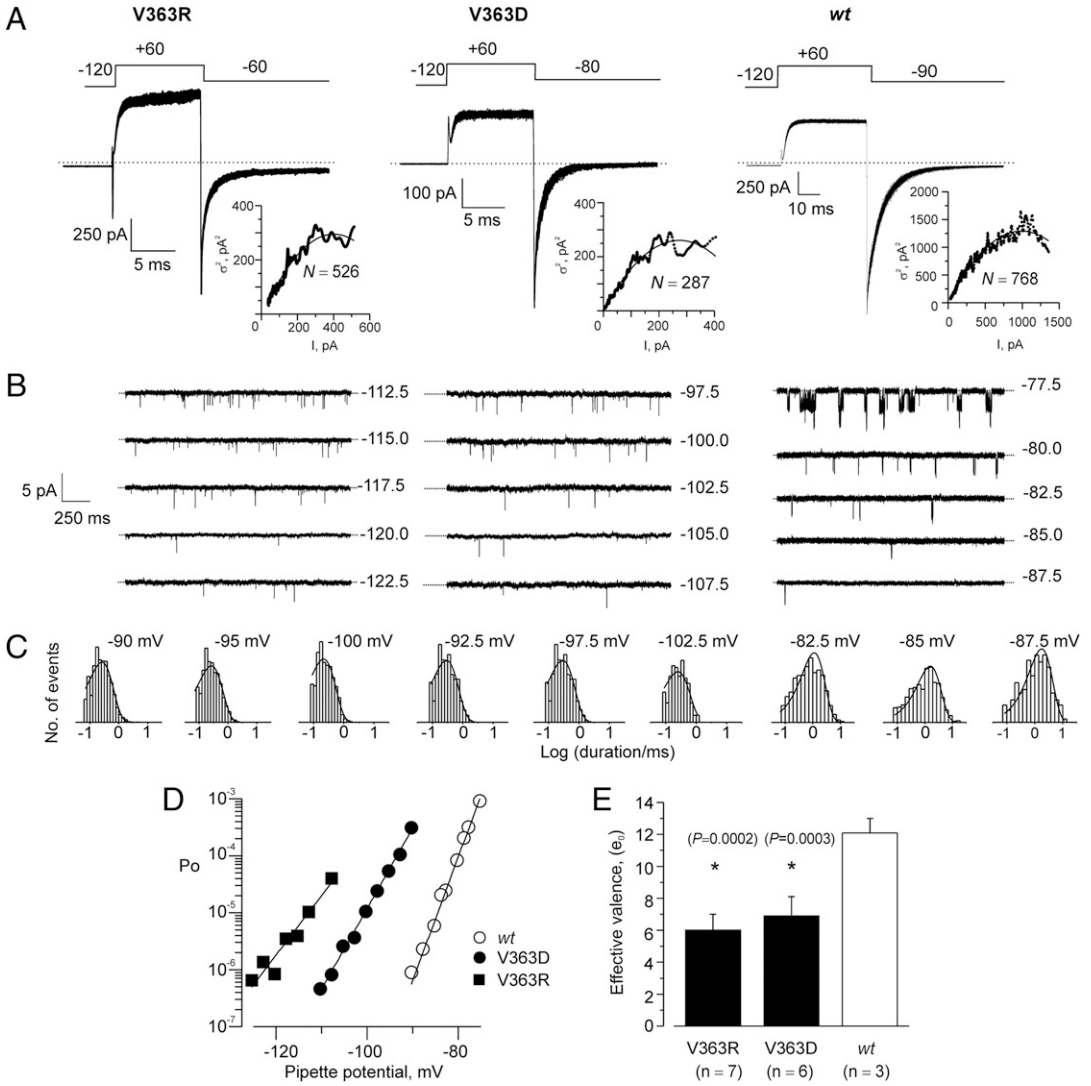

Fig. 2. Charged side chain at 363 decreases the valence of opening. (*A*) One hundred superimposed macroscopic current traces evoked by the protocols schematized at top. Each column corresponds to the channel construct specified at top. *Inset*: Nonstationary fluctuation analysis of the tail currents used to obtain the number of channels (*N*) (23). Continuous lines were drawn according to $\sigma^2(I) = C + (iI - I^2/N)$, where *i* is the unitary channel current. (*B*) Representative segments of 5-min records from the same patch shown in *A*. Opening are downward deflections. Voltage increments of 2.5 mV are shown at the right of each trace. (*C*) Three distributions of the open-duration events detected during 5 min at three different applied voltages. Voltages shown span 1 order of magnitude in Po. Solid line at the top of each distribution is the best maximum-likelihood single-exponential fit to logarithmically binned data. (*D*) Absolute Po (NPo/N) vs. V. Data points were fitted to the function $Po(V) = \exp(z_{lim}V/kT)$, where z_{lim} is the effective valence of opening. (*E*) Summary plot of z_{lim}. Results are means ± SD, and asterisks indicate significant differences from *wt* according to a two-tailed *t* test.

30 ms (short pulse; Fig. 4*A*) or 300 ms (long pulse; Fig. 4*B*). Application of MTSET produced distinctive time-dependent changes in current kinetics that were followed by plotting the amplitudes at the time indicated with vertical discontinuous lines over the traces (Fig. 4*C*). As expected, both R1C and R2C in the neutral 363 channels were modified faster in the higher-Po long-pulse protocols (Fig. 4*D*) (30, 31). Only for the charged variants of R1C (R1C/V363D and R1C/V363R), but not for those of R2C, did modification become faster and protocol independent, indicating a constitutively high solvent accessibility of this residue. These results support hypothesis *ii*: the charged side chains at 363 leave R1C, but not R2C, permanently exposed to the external solution.

How Large Is This Inward Displacement? The addition of charges at 363 may make S4 require more hydration, forcing water to creep deeper into the protein core. These extra water molecules would move inward the dielectric interface such that R1 gets permanently excluded from the electric field. Because the reduction in voltage sensitivity is independent of the charge sign at 363 (Fig. 2), this side chain must also be permanently outside the electric field, in contact with the external solution. The electrostatic potential originated by this charge must add locally to the electrical potential at the external interface and to the transmembrane voltage profile near S4 (Fig. 5*A*). In analogy with the surface charge effect, an extra charge, for example positive (Fig. 5*A*, *Left*), located near the interface would produce a positive potential (solid line) that locally increases the transmembrane voltage difference (dashed line). Conversely, an external negative charge would locally decrease the transmembrane voltage difference (Fig. 5*A*, *Right*). Thus, the near-symmetric shifts (around *wt*) along the voltage axis in the G-V relationships for V363D and V363R (Fig. 1*F*) are consistent with an electrostatic effect on the transmembrane potential. If, for simplicity, the negative and positive charges are equally separated from the interface, the observed gap of $\Delta V_{1/2} \approx$

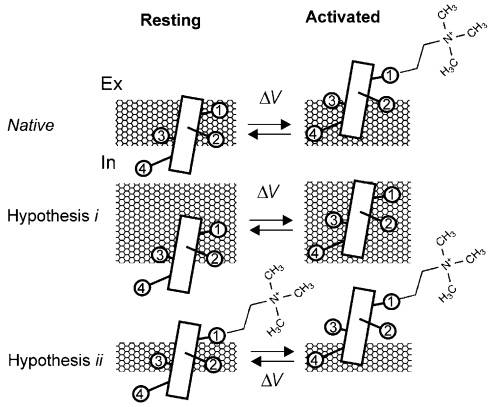

Fig. 3. Hypotheses involving reshaping of the electric field. (*Top*) In the *Native* channel, R1 (encircled number 1) is only accessible to modification by MTSET in the *Activated* conformation, and all sensing arginines (R1–R4) move across the electric field. (*Middle*) Hypothesis *i*: the charged side chain at 363 shifts the boundaries of the electric field outward. Then, R1 becomes inaccessible to MTSET at any activation state. All sensing arginines (R1–R4) move in the electric field but scan a smaller fraction of it, resulting in decreased voltage sensitivity. (*Bottom*) Hypothesis *ii*: the charged side chain at 363 shifts the boundaries of the electric field inward. Then, R1 becomes accessible to MTSET at any activation state. Some sensing arginines (R1–R4) do not move in the electric field, resulting in decreased voltage sensitivity.

28 mV between V363D and V363R G-V relationships would be equivalent to the difference in the local surface potential resulting from a charge reversion at 363. If the 363 charged side chain is in external solution, the observed $\Delta V_{1/2}$ gap should increase at lower external ionic strength because the electrostatic potential at the interface will be intensified by the reduced ionic screening. In separate paired experiments we observed that, in fact, the gap grew significantly from ≈30 to ≈40 mV after lowering ionic strength from $I = 0.11$ M to $I \approx 0.022$ M ($P = 0.0011$) (Fig. 5 *B* and *C*). From these experiments we estimated the separation of the charge at the 363 from the external border of the electric field using the Debye-Hückel theory. The change in potential ($\Delta\psi$), at a distance r, produced by a charge reversion is the difference between the potentials originated by the negative and the positive charges:

$$\Delta\psi(r) = \frac{2qe^{-r\kappa}}{4\pi\varepsilon\varepsilon_0 r},$$

where q is the charge size, ε and ε_0 are the dielectric constant and the vacuum permittivity. The constant κ is the reciprocal of the characteristic decay distance, the Debye-length, which decreases with the ionic strength, I, as $\kappa^{-1} = \sqrt{\frac{\varepsilon\varepsilon_0 RT}{2F^2 I}}$, where R and T and F have their usual meaning (32). I is defined as $I = 1/2 \cdot \sum n_i z_i^2$, where n_i and z_i are the molar concentration and valence of ionic species i in solution. For normal TEVC recording solution ($I \approx 0.11$ M), κ^{-1} ≈ 9.2 Å. Thus, a (±1) charge reversion would produce the observed $\Delta V_{1/2} \approx 30$ mV (Fig. 5*B*) if it is 6.2 Å away from the external border of the electric field ($\Delta\psi = 29.6$ mV). In agreement with the $\Delta V_{1/2} \approx$ 40 mV gap seen at $I \approx 0.022$ M (Fig. 5*C*), at $I = 0.022$ M, where κ^{-1} is 20.5 Å, a $\Delta\psi = 43$ mV is predicted 6.2 Å away. Thus, the charged side chain in 363 may reside in the aqueous solution, ≈6 Å away from the external dielectric boundaries.

Discussion

Ahern and Horn (16) showed that the modification with MTS-derived charged adducts of individual cysteines placed at several of the voltage-sensing and hydrophobic positions in Shaker S4

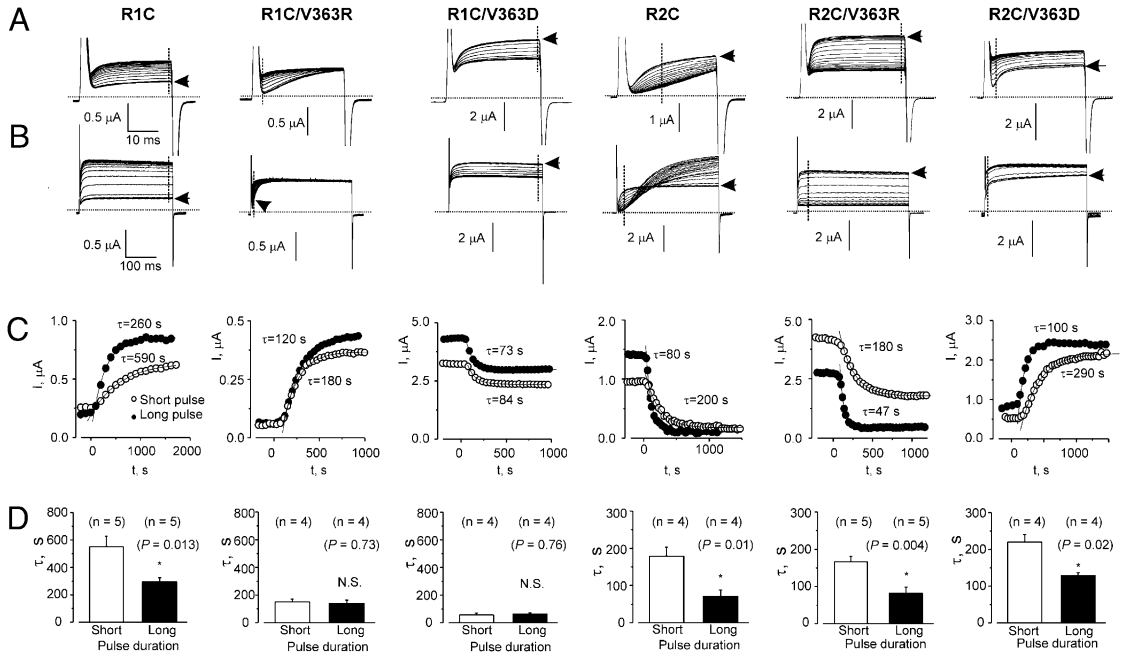

Fig. 4. Accessibility of R1C to extracellular MTSET becomes high and state-independent. (*A* and *B*) Representative K-current traces elicited in TEVC by short-pulse (*A*) and long-pulse (*B*) protocols differing in channel open duration by 10-fold. Arrows indicate the beginning of the external MTSET perfusion. (*C*) Time course plots of cysteine modification using short- or long-pulse protocols. Modification time course drawn by plotting current amplitudes at the times marked with the discontinuous vertical lines shown in *A* and *B*. Modification time courses were fitted to a single exponential function: $I(t) = I_0 + Ae^{-t/\tau}$, with τ value shown. (D) Time constants of modification using short- and long-pulse protocols. Results are means ± SD, and asterisks indicate significant differences ($P < 0.05$) between protocols according to a two-tailed *t* test. From these τ values the apparent second-order modification rate constants in the closed and open state, k_c and k_o respectively, were calculated in $mM^{-1}s^{-1}$ according to a procedure described previously (31). $k_c = 0.32$ and $k_o = 14.2$ for R1C; $k_{c/o} = 1.3$ for R1C/V363R; $k_{c/o} = 3.2$ for R1C/V363D; $k_c = 0.046$ and $k_o = 1.8$ for R2C; $k_c = 0.053$ and $k_o = 3.4$ for R2C/V363R; and $k_c = 0.041$ and $k_o = 0.7$ for R2C/V363D.

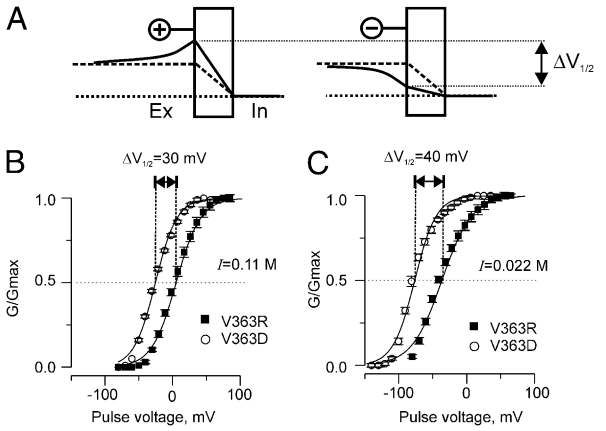

Fig. 5. Charged side chain at 363 influences the electrostatic field sensed by the voltage sensor. (*A*) Oppositely charged side chains affect the voltage profile across the membrane in opposite fashion. The transmembrane electric field (thick dashed line) is locally affected by nearby extracellular charges [represented by (+) and (–) "lollipops"]. According to the sign of the charge, the external border is made more positive or more negative (thick solid lines at right and left, respectively). The net difference between these opposite electrostatic effects corresponds to $\Delta V_{1/2}$. At lower ionic strength, the produced electrostatic field should be stronger, increasing $\Delta V_{1/2}$. (*B* and *C*) Voltage dependence of activation obtained at high and low ionic strength. G-V relationships were obtained in TEVC. Currents were first recorded in a normal-ionic-strength solutions (*B*; $I \approx 0.11$ M); then at low ionic strength (*C*; $I \approx 0.022$ M). Finally, a G-V curve was obtained at normal ionic strength to compare with those taken at the beginning. Only variations of $V_{1/2}$ <5 mV between the first and third recording were used. Data points were fitted to a simple Boltzmann distribution with parameters $V_{1/2}$ = 3.5 mV, z = 1.5 e_o for V363R in high ionic strength (n = 5); $V_{1/2}$ = −26.5, z = 1.62 e_o for V363D in high ionic strength (n = 6); $V_{1/2}$ = −38.8 mV, z = 1.26 e_o for V363R in low ionic strength; and $V_{1/2}$ = −78.6 mV, z = 1.74 e_o for V363D in low ionic strength.

(including Val363 and Ile364) revealed a dedicated architecture to carry charges across the electric field. R1, R2, and possibly R3 and R4 are the only positions to which charged adducts altered the total gating charge according to their sign. In contrast to this clear trend, positive charge introduction to positions between R1 and R2 reduced the charge per channel, whereas negatively charged modification at 364 did not change the size of the charge. Here, both negative and positive charges at 363 or 364 reduced voltage dependence. Considering that the limiting slope method only measures the charge linked to channel opening, the relatively good agreement with the Ahern and Horn measures is satisfying. A disagreement on 364 could be expected if the 364C background used by the authors already exhibited a reduced charge per channel. We speculate that a negative adduct would not further reduce the charge per channel if a significant fraction of the 364C sulfhydryl, perhaps with pK_a <8.3, is already ionized.

We propose that the additional charge in the 363 variants is unable to move across the electric field. Moreover, the side chain at 362 (R1) is also unable to cross the field. Experiments outlined in Figs. 3 and 4 show that residue 362, which is buried in the resting native channel, became permanently solvent accessible in the charged 363 variant. However, R1 and S4 move normally in these variants, because (*i*) the charged mutant channels open with similar maximal Po to a single open state population (Fig. 2 *A* and *C*), thus the access to the fully active S4 conformation may not be affected; (*ii*) although constitutively exposed, residue R1C retained its ability to shuttle between S1-241 and S5-419; both S1-241C and S5-419C mutants were able to coordinate Cd^{2+} (Fig. S3); and (*iii*) accessibility of residue 365 to MTS in the charged variants remained as much activation dependent as in the uncharged ones, retaining the magnitudes of the modification rates (see Fig. 4 legend). Thus, the activation path for R2 is preserved too. We maintain that the charge addition at V363 moves the solvent-accessible boundaries at least ≈6 Å inward. Thus, we explain the reduction in the voltage dependency, because R1 movement does not cross the electric field, as depicted in Fig. 3.

Charge Hydration May Define the Electric Field Boundaries. Molecular simulations show charged side chains near the core of transmembrane α-helices surrounded by water, forming a local microscopic polar environment (7, 33). Consistent with this, VSD reconstituted in phospholipids seems highly hydrated when compared with a typical hydrophobic transmembrane segment (4, 18). Molecular simulations of the VSD of Kv1.2 channels embedded in phospholipid bilayers show hydration water molecules surrounding S4 arginines (5, 6). Thus, charges attract water deeper into the membrane plane, shaping the dielectric boundaries and possibly the electric field (4). Alternatively, S4 arginines in voltage-gated ion channels may be tolerated in the core of the membrane by making direct, specific contacts with the phospholipids phosphate groups (11, 13, 14, 25). Our results are inconsistent with this view, supporting the idea that the charge itself, more than its sign, shapes protein contacts. In the open Kv1.2-Kv2.1 channel chimera (10), the side chain of Leu294 (equivalent to Shaker-Val363) contacts surrounding lipidic-acyl chains (Fig. 1*B*). A charged side chain in that position would replace those contacts with water molecules.

Few Charges in the Electric Field. The charge at the 363 side chain is ≈6 Å apart from the low dielectric-water interface (Fig. 5). If R2 (R2C in Fig. 4) is buried at rest, then the side chain of 363 must be separated by at least 6 Å from this residue. Assuming that 363 lies between R1 and R2, 6 Å could be a lower limit for the R1–R2 intercharge distance. Arising from the Debye-Hückel theory, the calculation is a bit gross because we assumed the tethered charge as being fully immersed in the aqueous solution and projecting a spherical field with no microscopic graininess. Although this charge separation could be underestimated if the charged side chain lies at the dielectric interface (34) or in a water cavity (35), this type of calculation has previously proven to be accurate to describe nearby electrostatic influence on the voltage sensor (34, 36, 37). Because this 6-Å separation compares well with the crystallographic separation between R1 and R2 guanidinium groups (9, 10) and is similar to or larger than the estimated 3–7-Å thickness of the low dielectric septum traversed by the charges during activation (36, 38), at most a single sensing arginine side chain could be found within the field. But, from an energetic point of view, the guanidinium groups would be found hydrated rather than within the septum. If the S4 segment has a periodic structure, this estimated charge separation could be applied for all four sensing arginines.

Optimized Voltage Sensitivity. Considering the high conservation of the hydrophobic nature of the side chain at 363 and the other charge spacing hydrophobic residues of S4 in voltage-gated Na^+ and K^+ channels (17, 18, 39), the low energetic impact on the open–closed equilibrium caused by the dramatic change in the nature of 363 side chain (Fig. 1*F*) argues against a structural value for such high conservation. In fact, as shown here and suggested in ref. 16, the hydrophobic nature of this residue may play a role in shaping the water–lipid boundaries (Figs. 1*B* and 4). Several point mutations in S4 shunt the electric field, transforming the VSD into a cationic channel (27, 40–42), indicating that the low dielectric septum can easily be disorganized. The array of regularly spaced arginines and hydrophobic residues in S4 would be optimized to sustain high voltage sensitivity for neuronal K^+ and Na^+ channels, where arginine positions are dedicated to sensing the voltage (16) whereas the hydrophobic residues shape the electric field. Additional positive charges in S4 would not increase voltage sensitivity

because they would drag water molecules deeper, moving the boundaries of the electric field, thereby reducing the effective valence of activation or disorganizing the septum.

Materials and Methods

Molecular Biology. Salts were from Sigma-Aldrich, MTSET from Toronto Chemicals, and charybdotoxin from Alomone Labs. Standard techniques were used; we only detail specific modifications. All point mutations were introduced in a background N-inactivation deficient Shaker K-channel having a 1,000-fold enhanced sensitivity for charybdotoxin (19) and verified by sequencing (Macrogen). In vitro synthesis of cRNA was carried out with the Message Machine kit (Ambion) according to the manufacturer's instructions. *Xenopus laevis* care, surgery, and oocytes preparation are described elsewhere (20). DTT (0.1 mM) was added to the oocyte incubation solution after cRNA injection for MTSET accessibility experiments. For whole-oocyte recordings, cRNA injected was 0.5–2 ng, and 2–5 ng for both cut-open oocyte and cell-attached patch-clamp recordings.

Electrophysiology. For TEVC, oocytes were impaled with two 3M KCl-filled capillary Ag/AgCl electrodes with resistances in the 0.2–1.0 MΩ (20) range. Current recording were performed with an OC-725C amplifier (Warner Instruments) through a PCI-6035 interface (National Instruments) under the command of WinWCP software (Strathclyde University). Normal recording solution (in mM) was 100 NaCl, 2.5 KCl, 1.8 $CaCl_2$, 1 $MgCl_2$, and 10 Hepes-NaOH (pH 7.4). The low-ionic-strength recording solution (0.022 M) was (in mM) 6 NaCl, 0.5 KCl, 1.8 $CaCl_2$, 1 $MgCl_2$, 180 Sucrose, and 10 Hepes-NaOH (pH 7.4). Freshly dissolved 5 μM MTSET was added to the recording solution for state dependency of R1C, whereas for R2C, 100 μM MTSET was used. For cut-open oocyte voltage clamp, current recording were performed with a Dagan 1B amplifier (Dagan Instruments) through a Digidata 1200B interface with pClamp 8.0 software (Molecular Devices). Gating currents were recorded after allowing >30 min for equilibration with this internal solution (in mM): 120 NMG-Mes, 0.1 EGTA, and 10 Hepes (pH 7.4). The external, and guard, solution was composed of (in mM) 120 NMG-Mes, 2 $CaMES_2$, 1 $MgCl_2$, and 10 Hepes (pH 7.4) plus 1 μM charybdotoxin. For cell-attached patch-clamp, pipette electrodes were made from aluminum-silicate (Sutter Instruments) and fire-polished to resistances between 0.5 and 2 MΩ. The tip was covered with Sylgard (Sigma-Aldrich) for improved noise response. Electrodes were filled with (in mM) 110 KMES, 2 $CaCl_2$, and 10 Hepes (pH 7.4), whereas the bath had (in mM) 110 KMES, 2 $MgCl_2$, 0.1 EGTA, and 10 Hepes (pH 7.4). Before forming the high-resistance seal, oocytes were mechanically broken to equilibrate the intracellular environment with the bath solution. Ionic currents were recorded with an Axopatch 200B amplifier through a Digidata 1440 interface running under pClamp 10 (Molecular Devices). Current traces were filtered to 5 kHz with a Bessel and acquired at 50 kHz. For off-line analysis traces were Gaussian refiltered to 2 kHz with pClamp. Single-channel event durations were measured with the 50% threshold method. No correction for missed events was attempted, provided that Po would be equally distorted at any voltage. *N*Po was calculated from the fractional time at levels corresponding to 0, 1, 2, ...*n* open channels approximated to a Poisson distribution.

The electrostatic contribution of the additional charge to the electric field was calculated with the Debye-Hückel theory. This theory describes how the potential (ψ) originated by a point charge attenuates in salt solutions in mV (35): $\psi(r) = \frac{180ze^{-r\kappa}}{r}$, where r is the distance in Å from the charge, z is the valence, and κ is the reciprocal of the Debye-length, which decreases with the ionic strength (I, in M) as: $\kappa^{-1} = \frac{3.044}{\sqrt{I}}$.

ACKNOWLEDGMENTS. We thank V. Prado and T. Estévez for technical help; and Alan Neely, Ramón Latorre, and John Ewer for critical reading. This work was partly funded by Programa Bicentenario ACT-46 and Fondo Nacional de Desarrollo Científico y Tecnológico (FONDECYT) 1090493. V.G.P. and K.B. were doctoral fellows of Comision Nacional de Investigación Científica y Tecnológica (CONICYT).

1. Aggarwal SK, MacKinnon R (1996) Contribution of the S4 segment to gating charge in the Shaker K+ channel. *Neuron* 16:1169–1177.
2. Seoh SA, Sigg D, Papazian DM, Bezanilla F (1996) Voltage-sensing residues in the S2 and S4 segments of the Shaker K+ channel. *Neuron* 16:1159–1167.
3. Bezanilla F (2008) How membrane proteins sense voltage. *Nat Rev Mol Cell Biol* 9: 323–332.
4. Krepkiy D, et al. (2009) Structure and hydration of membranes embedded with voltage-sensing domains. *Nature* 462:473–479.
5. Jogini V, Roux B (2007) Dynamics of the Kv1.2 voltage-gated K+ channel in a membrane environment. *Biophys J* 93:3070–3082.
6. Treptow W, Tarek M (2006) Environment of the gating charges in the Kv1.2 Shaker potassium channel. *Biophys J* 90:L64–L66.
7. Johansson AC, Lindahl E (2006) Amino-acid solvation structure in transmembrane helices from molecular dynamics simulations. *Biophys J* 91:4450–4463.
8. Tiwari-Woodruff SK, Schulteis CT, Mock AF, Papazian DM (1997) Electrostatic interactions between transmembrane segments mediate folding of Shaker K+ channel subunits. *Biophys J* 72:1489–1500.
9. Long SB, Campbell EB, Mackinnon R (2005) Crystal structure of a mammalian voltage-dependent Shaker family K+ channel. *Science* 309:897–903.
10. Long SB, Tao X, Campbell EB, MacKinnon R (2007) Atomic structure of a voltage-dependent K+ channel in a lipid membrane-like environment. *Nature* 450:376–382.
11. Xu Y, Ramu Y, Lu Z (2008) Removal of phospho-head groups of membrane lipids immobilizes voltage sensors of K+ channels. *Nature* 451:826–829.
12. Ramu Y, Xu Y, Lu Z (2006) Enzymatic activation of voltage-gated potassium channels. *Nature* 442:696–699.
13. Hessa T, White SH, von Heijne G (2005) Membrane insertion of a potassium-channel voltage sensor. *Science* 307:1427.
14. Schmidt D, Jiang QX, MacKinnon R (2006) Phospholipids and the origin of cationic gating charges in voltage sensors. *Nature* 444:775–779.
15. Mackinnon R (2005) Structural biology. Membrane protein insertion and stability. *Science* 307:1425–1426.
16. Ahern CA, Horn R (2004) Specificity of charge-carrying residues in the voltage sensor of potassium channels. *J Gen Physiol* 123:205–216.
17. Lee SY, Banerjee A, MacKinnon R (2009) Two separate interfaces between the voltage sensor and pore are required for the function of voltage-dependent K(+) channels. *PLoS Biol* 7:e47.
18. Chakrapani S, Cuello LG, Cortes DM, Perozo E (2008) Structural dynamics of an isolated voltage-sensor domain in a lipid bilayer. *Structure* 16:398–409.
19. Goldstein SA, Miller C (1992) A point mutation in a Shaker K+ channel changes its charybdotoxin binding site from low to high affinity. *Biophys J* 62:5–7.
20. González-Pérez V, et al. (2008) Slow inactivation in Shaker K channels is delayed by intracellular tetraethylammonium. *J Gen Physiol* 132:633–650.
21. Islas LD, Sigworth FJ (1999) Voltage sensitivity and gating charge in Shaker and Shab family potassium channels. *J Gen Physiol* 114:723–742.
22. Hirschberg B, Rovner A, Lieberman M, Patlak J (1995) Transfer of twelve charges is needed to open skeletal muscle Na+ channels. *J Gen Physiol* 106:1053–1068.
23. Schoppa NE, McCormack K, Tanouye MA, Sigworth FJ (1992) The size of gating charge in wild-type and mutant Shaker potassium channels. *Science* 255:1712–1715.
24. Almers W (1978) Gating currents and charge movements in excitable membranes. *Rev Physiol Biochem Pharmacol* 82:96–190.
25. Jiang Y, Ruta V, Chen J, Lee A, MacKinnon R (2003) The principle of gating charge movement in a voltage-dependent K+ channel. *Nature* 423:42–48.
26. Horn R (2002) Coupled movements in voltage-gated ion channels. *J Gen Physiol* 120: 449–453.
27. Campos FV, Chanda B, Roux B, Bezanilla F (2007) Two atomic constraints unambiguously position the S4 segment relative to S1 and S2 segments in the closed state of Shaker K channel. *Proc Natl Acad Sci USA* 104:7904–7909.
28. Long SB, Campbell EB, Mackinnon R (2005) Voltage sensor of Kv1.2: Structural basis of electromechanical coupling. *Science* 309:903–908.
29. Lainé M, et al. (2003) Atomic proximity between S4 segment and pore domain in Shaker potassium channels. *Neuron* 39:467–481.
30. Yang N, George AL, Jr, Horn R (1996) Molecular basis of charge movement in voltage-gated sodium channels. *Neuron* 16:113–122.
31. Larsson HP, Baker OS, Dhillon DS, Isacoff EY (1996) Transmembrane movement of the shaker K+ channel S4. *Neuron* 16:387–397.
32. Bergethon PR, Simons ER (1990) *Biophysical Chemistry: Molecules to Membranes* (Springer-Verlag, New York), pp xiv.
33. White SH (2009) Biophysical dissection of membrane proteins. *Nature* 459:344–346.
34. Broomand A, Elinder F (2008) Large-scale movement within the voltage-sensor paddle of a potassium channel-support for a helical-screw motion. *Neuron* 59: 770–777.
35. Hille B (2001) *Ion Channels of Excitable Membranes* (Sinauer, Sunderland, MA), , 3rd Ed, pp 545–547.
36. Islas LD, Sigworth FJ (2001) Electrostatics and the gating pore of Shaker potassium channels. *J Gen Physiol* 117:69–89.
37. Elinder F, Arhem P, Larsson HP (2001) Localization of the extracellular end of the voltage sensor S4 in a potassium channel. *Biophys J* 80:1802–1809.
38. Ahern CA, Horn R (2005) Focused electric field across the voltage sensor of potassium channels. *Neuron* 48:25–29.
39. Guda P, Bourne PE, Guda C (2007) Conserved motifs in voltage-sensing and pore-forming modules of voltage-gated ion channel proteins. *Biochem Biophys Res Commun* 352:292–298.
40. Starace DM, Bezanilla F (2004) A proton pore in a potassium channel voltage sensor reveals a focused electric field. *Nature* 427:548–553.
41. Sokolov S, Scheuer T, Catterall WA (2007) Gating pore current in an inherited ion channelopathy. *Nature* 446:76–78.
42. Tombola F, Pathak MM, Isacoff EY (2005) Voltage-sensing arginines in a potassium channel permeate and occlude cation-selective pores. *Neuron* 45:379–388.